JCI insight

Combination of PD-L1 and PVR determines sensitivity to PD-1 blockade

Bo Ryeong Lee, … , Hye Ryun Kim, Sang-Jun Ha

JCI Insight. 2020;5(14):e128633. https://doi.org/10.1172/jci.insight.128633.

Research Article | Immunology | Oncology

Graphical abstract

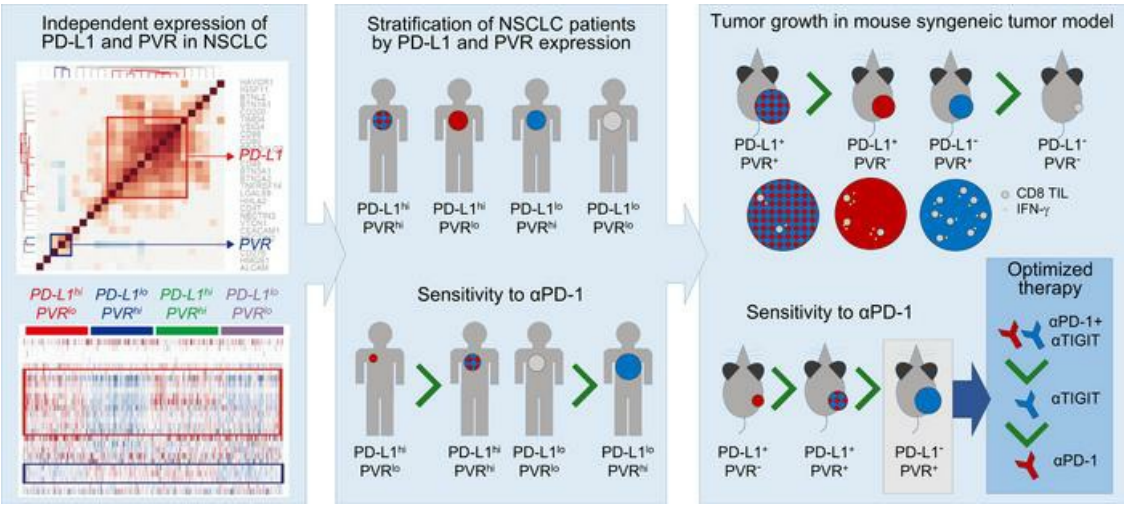

Find the latest version:

https://jci.me/128633/pdf

JCI insight

RESEARCH ARTICLE

Combination of PD-L1 and PVR determines sensitivity to PD-1 blockade

Bo Ryeong Lee,[1,2] Sehyun Chae,[3] Jihyun Moon,[1,2] Myeong Joon Kim,[1,2] Hankyu Lee,[1,2] Hyuk Wan Ko,[1,2] Byoung Chul Cho,[4] Hyo Sup Shim,[5] Daehee Hwang,[6] Hye Ryun Kim,[4] and Sang-Jun Ha[1,2]

[1]Department of Biochemistry, College of Life Science & Biotechnology, and [2]Brain Korea 21 (BK21) PLUS Program, Initiative for Biological Functions & Systems, Yonsei University, Seoul, Republic of Korea. [3]Korea Brain Bank, Korea Brain Research Institute, Daegu, Republic of Korea. [4]Yonsei Cancer Center, Division of Medical Oncology, and [5]Department of Pathology, Yonsei University College of Medicine, Seoul, Republic of Korea. [6]Department of Biological Sciences, Seoul National University, Seoul, Republic of Korea.

Expression of immune checkpoint ligands (ICLs) is necessary to trigger the inhibitory signal via immune checkpoint receptors (ICRs) in exhausted T cells under tumor immune microenvironment. Nevertheless,to our knowledge, ICL expression profile in cancer patients has not been investigated. Using previously reported RNA-seq data sets, we found that expression of ICLs was patient specific but their coexpression can be patterned in non–small-cell lung cancers (NSCLCs). Since the expression of PD-L1 and poliovirus receptor (PVR) among various ICLs was independently regulated, we could stratify the patients who were treated with anti–PD-1 later into 4 groups according to the expression level of PD-L1 and PVR. Of interest, high PVR and low PVR expressions in PD-L1–expressing patients enriched nonresponders and responders to PD-1 blockade, respectively, helping in further selection of responders. Using a genetically engineered cancer model, we also found that PVR-deficient and PD-L1–sufficient tumor-bearing mice were highly sensitive to anti–PD-1 therapy, whereas PVR-sufficient and PD-L1–deficient tumor-bearing mice were resistant to anti–PD-1 therapy. Taken together, our study provides a concept that combinatorial expression patterns of PVR and PD-L1 are key determinants for PD-1 blockade and furthermore suggest a better therapeutic usage of immune checkpoint blockades (ICBs).

Introduction

Cancer cells adopt mechanisms to evade immune surveillance (1). In particular, inhibitory checkpoint pathways that suppress the antitumor activity of T cells are frequently found in the tumor microenvironment (TME). Immune checkpoint blockade (ICB) anti–programmed cell death-1 (anti–PD-1) therapy has been proven to show durable responses and improved survival rates in patients with multiple types of cancer, including non–small-cell lung cancer (NSCLC) (2). Despite its encouraging efficacy, only about 30% of NSCLC patients respond to anti–PD-1 therapy (3). To maximize the therapeutic benefits of this treatment, as well as minimize the risk of immune-related adverse effects (irAE), there is a significant need for robust biomarkers that can be used to improve the selection of patients for personalized therapy.

Programmed cell death ligand-1 (PD-L1) is a ligand of PD-1, the binding of which triggers the transduction of inhibitory signals (4). Thus, it has been approved as a biomarker for anti–PD-1 therapy in patients with NSCLC. Many studies have shown that PD-L1 expression is enriched in the responders to anti–PD-1 therapy. However, a significant proportion of PD-L1$^+$ patients still show no response to therapy, and a subset of PD-L1$^-$ patients are in fact responsive to treatment (5, 6). To overcome the limitations of PD-L1 as a biomarker, other factors associated with CD8$^+$ T cell infiltration, intestinal microbiota, and tumor mutational load have been studied (7–9). However, these were not sufficient to achieve a reliable prediction of patient sensitivity to anti–PD-1 therapy.

Other immune checkpoint pathways that suppress T cells in the TME exist in addition to the PD-1 pathway (10, 11). Similar to exhausted T cells in chronic infection models, T cells in the TME express multiple immune checkpoint receptors (ICRs) — including PD-1, T cell immunoglobulin mucin-3 (TIM-3), and T cell immunoreceptor with Ig and ITIM domains (TIGIT) — in various tumor types, and coblockade of these receptors show synergistic effects on the expansion and anti-tumor function of CD8$^+$ T cells (12–15). Recently, these receptors

Authorship note: BRL, SC, and JM contributed equally to this work.

Conflict of interest: SJH, HRK, DH, and BRL have patent pertaining to the results presented in the paper (patent no.10-2084196 Korea).

Submitted: March 6, 2019
Accepted: June 4, 2020
Published: July 23, 2020.

Reference information: *JCI Insight*. 2020;5(14):e128633. https://doi.org/10.1172/jci.insight.128633.

were found to be coexpressed as a coinhibitory gene regulatory program at single-cell resolution (16). Accordingly, the expression patterns of their corresponding ligands could be of clinical relevance to indicate the type of immune checkpoint pathways that patients possess in their tumors. However, the expression patterns of the ligands and the prevalence of their expression in lung cancer patients have not yet been extensively analyzed.

Here, we investigate the coexpression patterns of immune checkpoint ligands (ICLs) in 5 different cohorts of lung adenocarcinoma patients, including The Cancer Genome Atlas (TCGA) cohort, using their mRNA gene expression profiles. Among these ICLs, we found that poliovirus receptor (*PVR*), a ligand of TIGIT, showed virtually no correlation to *PD-L1* in its expression pattern across tumors; thus, the complementary expression pattern of PD-L1 and PVR could be used to predict responders to PD-1 blockade in NSCLC patients. Furthermore, using a mouse tumor model, we found a reciprocal association between PD-L1 and PVR expression and sensitivity to anti-TIGIT and anti–PD-1 therapies, respectively, and we confirmed the clinical value of the combinatorial expression pattern of PD-L1 and PVR as an indicator that can afford patient stratification for personalized ICB therapy.

Results

PVR is expressed independently of PD-L1 in 5 different lung adenocarcinoma cohorts. Although several studies have investigated the coexpression patterns of ICRs in different types of cancer, the coexpression patterns of ICLs have been addressed relatively less. To explore the coexpression patterns of ICLs, we analyzed correlations between expression levels in 27 ICLs using the following gene expression profiles obtained from 5 different cohorts of lung adenocarcinoma (LUAD) patients: TCGA-LUAD RNA sequencing (RNA-seq) data (17) from the TCGA database, and GSE30219 (18), GSE37745 (19), GSE31210 (20), and GSE10245 (21) microarray data sets from the gene expression omnibus database. We first analyzed the correlations among ICLs in the TCGA database (Figure 1A) and the other individual data sets (Supplemental Figure 1A; supplemental material available online with this article; https://doi.org/10.1172/jci.insight.128633DS1) individually, and we then combined them into representative correlations using the Schmidt–Hunter method (22) (Supplemental Figure 1B). Clustering analysis of these correlations revealed the largest *PD-L1* (*CD274*) cluster (red box in Figsure 1A and Supplemental Figure 1, A and B), which includes *PD-L1* and 10 other ICLs (*CD48*/*80*/*86*, *BTN2A2*/*3A1*, *TIMD4*, *VSIG4*, *PDCD1LG2*, *TNFRSF14*, and *LGALS9*), and a *PVR* cluster, which includes *PVR*, *NECTIN2*, and *CD276*, with virtually no correlations or even anticorrelation with the ICLs of the *PD-L1* cluster (blue box in Figure 1A; and Supplemental Figure 1, A and B). Unlike these ICLs, however, the correlation analysis of their known ICRs did not reveal an independent correlation pattern between these *PD-L1* and *PVR* clusters (e.g., *PD-1* [*PDCD1*] and *TIGIT* for *PD-L1* and *PVR*, respectively), but it showed strong correlations between the expression levels of all ICRs (Figure 1B and Supplemental Figure 1C).

To comprehensively visualize individual ICL expression, we categorized the patients into 4 groups: (a) high expression of *CD274* and *PVR* (hi/hi); (b) low expression of *CD274* and high expression of *PVR* (lo/hi); (c) high expression of *CD274* and low expression of *PVR* (hi/lo); and (d) low expression of *CD274* and *PVR* (lo/lo). The expression of *PD-L1* and *PVR* in individual patients categorized into 4 groups also revealed that they are independently expressed (Figure 1C and Supplemental Figure 1D). Moreover, we investigated the contribution of *CD274* and *PVR* to the prognosis by analyzing the survival difference between 2 patient groups with high ($\geq 50^{th}$ percentile) and low ($< 50^{th}$ percentile) levels of ICL expression using 2 (TCGA and GSE31210, respectively) of the 5 cohorts, consisting of more than 200 patients, to ensure statistical power. High expression of *PVR* was strongly associated with poor prognostic, and that of *CD274* also tend to be despite weak significance (Figure 1D). According to the multivariate survival analysis of 4 groups, the hi/hi group showed the poorest survival rates compared with the other groups, suggesting the synergistic effect of PD-L1 and PVR on prognosis (Figure 1D).

Furthermore, the *PD-L1* and *PVR* clusters were also consistently observed in other major types of cancers in TCGA, including lung squamous cell carcinoma, glioblastoma, melanoma, colon adenocarcinoma, and head and neck, ovarian, bladder, and breast cancers (Figure 1E and Supplemental Figure 1E). Consequently, we identified *PVR* as an independently expressed ICL with *CD274* so we could categorize patients based on the expression of *CD274* and *PVR*.

The use of both PD-L1 and PVR expression improves the prediction accuracy of responders to anti–PD-1 therapy in NSCLC patients. To determine whether the identified pair of ICLs, PD-L1, and PVR show similar independent expression patterns at the protein level, tumor specimens from 96 NSCLC patients who had undergone anti–PD-1 or anti–PD-L1 therapy were used as a discovery set. We analyzed the expression

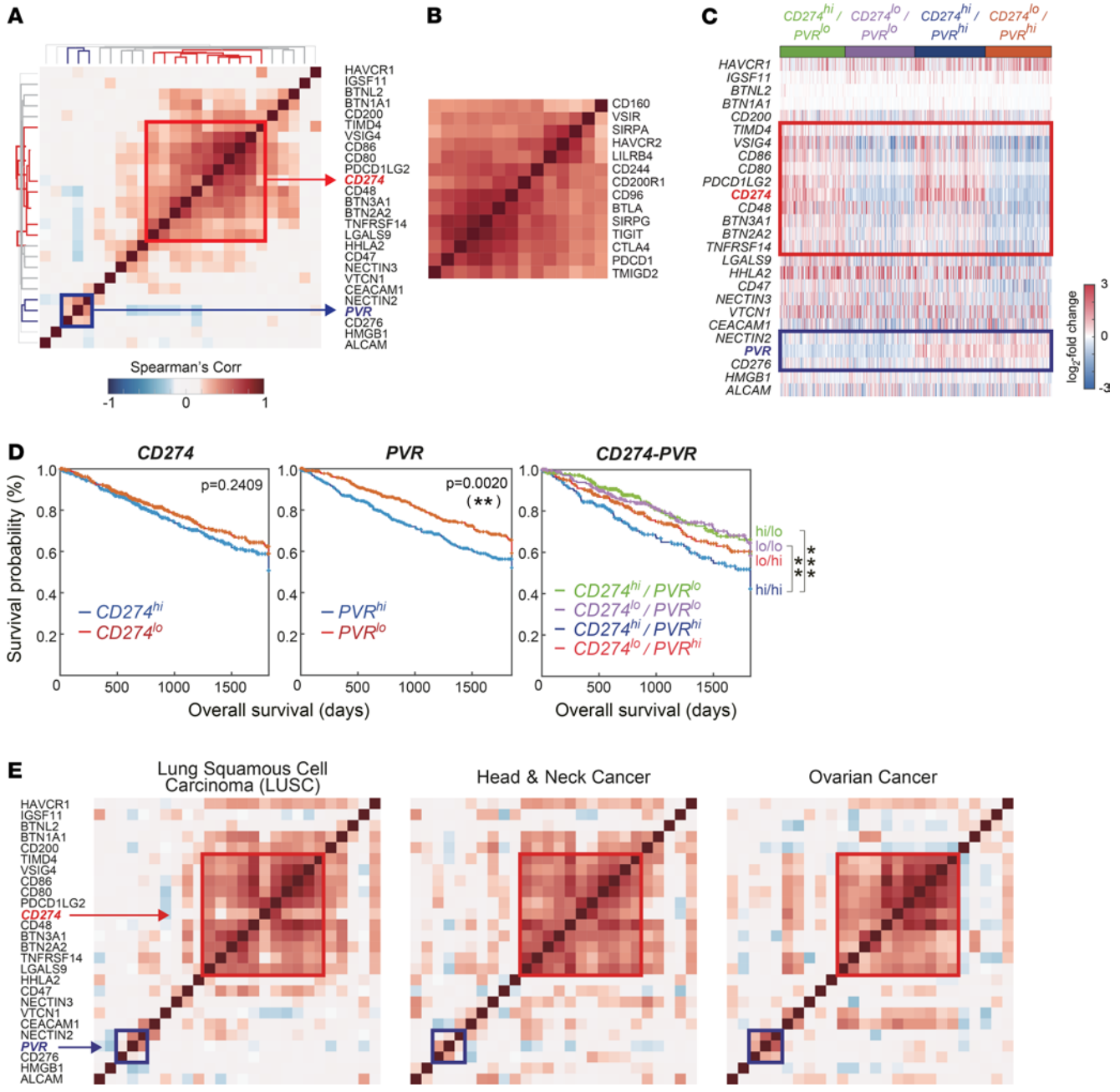

Figure 1. PVR is expressed independently of PD-L1. (**A** and **B**) Correlation analysis of expression levels of 27 ICLs (**A**) and 14 ICRs (**B**) in lung adenocarcinoma from TCGA database. The heatmap shows Spearman's correlation coefficients for all pairs of ICLs. The dendrogram shows the result from hierarchical clustering of the ICLs based on the correlation coefficients using Euclidean distance as a dissimilarity measure and single linkage method. Red and blue branches in the dendrogram represent the PD-L1 (CD274, red box) and PVR (blue box) clusters, respectively. (**C**) Gene expression patterns of the ICLs in 4 patient groups ($CD274^{hi}/PVR^{lo}$, $CD274^{lo}/PVR^{lo}$, $CD274^{hi}/PVR^{hi}$, and $CD274^{lo}/PVR^{hi}$) in the TCGA-LUAD data set. Red and blue colors represent increased and decreased expression levels of each ICL, respectively, with respect to its median expression level. The color bar denotes the gradient of $\log_2$ fold-changes of expression levels in individual samples with respect to its median expression level. (**D**) Kaplan–Meier survival analysis of 2 patient groups with high (blue) and low (red) expression levels of *CD274* (left) or *PVR* (right), respectively. $^{**}P < 0.01$ according to the Wilcoxon test. Multivariate survival analysis of 4 patient groups - $CD274^{hi}/PVR^{lo}$ (green), $CD274^{lo}/PVR^{lo}$ (purple), $CD274^{hi}/PVR^{hi}$ (blue) and $CD274^{lo}/PVR^{hi}$ (red). $^{**}P < 0.01$ and $^{***}P < 0.001$ by Multivariate Wilcoxon with multiple comparison test. (**E**) Correlation patterns of 27 ICLs in 3 TCGA major cancers, lung squamous cell carcinoma (left), head and neck cancer (middle), and ovarian cancer (right).

for PD-L1 and PVR proteins in the tumors using IHC (Figure 2A). PVR expression was scored as the percentage of membranous staining on tumor cells (Figure 2A, bottom), as in the PD-L1 IHC scoring method (23). The distributions of PD-L1 and PVR TPSs showed that the median values of PD-L1 and PVR were 10% and 60%, respectively (Supplemental Figure 2, A and B). To facilitate the stratification

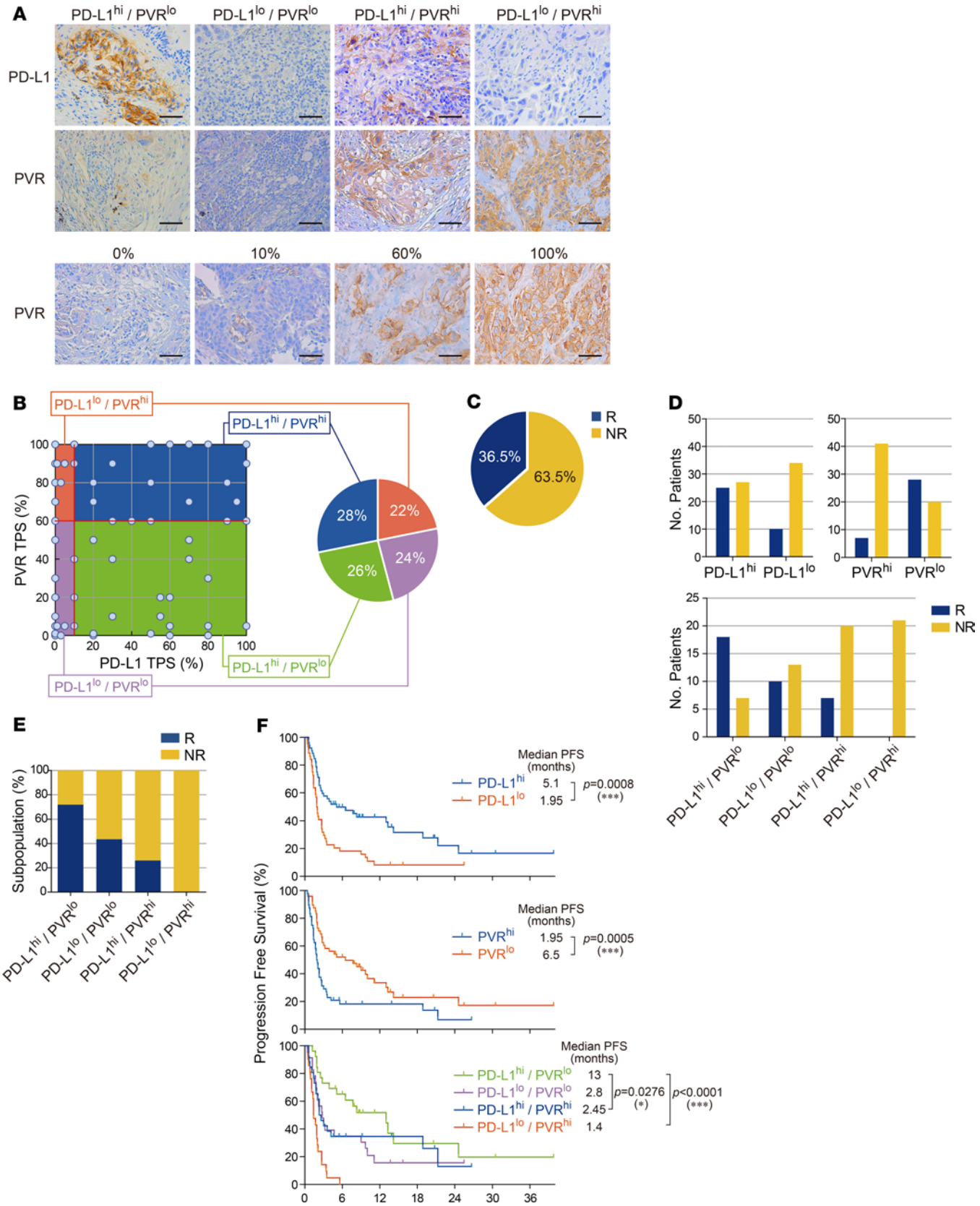

Figure 2. The use of both PD-L1 and PVR expression improves the prediction accuracy of responders to anti–PD-1 therapy in NSCLC patients. (**A**) Representative images (400×) of PD-L1 and PVR IHC staining of tumors from patients with NSCLC. Scale bars: 50 μm. (**B**) Prevalence of PD-L1 and PVR IHC staining patterns in tumors from patients with NSCLC (n = 96); each dot indicates 1 patient. Red lines indicate the median tumor proportion scores (TPSs) of PD-L1 and PVR (10 and 60, respectively), which divide PD-L1^{hi}PD-L1^{lo} and PVR^{hi}/PVR^{lo} patients. (**C**) Pie chart depicting the overall objective response rate

(ORR) of NSCLC patients enrolled in anti–PD-1 therapy. (**D**) Number of responding or nonresponding patients for anti–PD-1 therapy by PD-L1 or/and PVR above or below the median. (**E**) ORR by PD-L1 and PVR expression each above or below the median. Blue, responders (R); yellow, nonresponders (NR). (**F**) Kaplan–Meier plots of progression-free survival (PFS) by PD-L1 or/and PVR expression above or below the median for anti–PD-1 therapy. $*P < 0.05$ and $***P < 0.001$ by Wilcoxon test or multivariate Wilcoxon with multiple comparison test.

of patients according to the protein expressions of PD-L1 and PVR, we set the cutoff for the expressions of PD-L1 and of PVR in tumors as their median values and then defined the patients with tumors of values ≥ cutoff as "high" (≥ 10% and ≥ 60% for PD-L1 and PVR, respectively) and the others as "low." By using the definition for PD-L1 and PVR expression levels in tumors, we could categorize the patients into 4 different groups (Figure 2A). Of interest, the patients seemed to be evenly distributed in 4 groups: PD-L1^{lo}PVR^{hi} (21 of 96, 22%), PD-L1^{lo}PVR^{lo} (23 of 96, 24%), PD-L1^{hi}PVR^{lo} (25/96, 26%), and PD-L1^{hi}PVR^{hi} (27 of 96, 28%) (Figure 2B), confirming the result that showed the independent mRNA expressions of *CD274* and *PVR* and no expression correlation between 2 genes. There were no significant differences in the clinicopathological characteristics among these groups (Table 1).

Next, we examined whether these 4 groups could show distinct responsiveness to anti–PD-1 or anti–PD-L1 therapy. The responders who showed partial response (PR) or stable disease (SD) lasting longer than 6 months of the above 96 patients after PD-1 blockade were found to be 36.5% (35 of 96) (Figure 2C). While PD-L1^{hi} group enriched responders compared with PD-L1^{lo} group (48.1% [25 of 52] vs. 22.7% [10 of 44], $P = 0.01$), the PVR^{hi} group enriched nonresponders compared with PVR^{lo} group (85.4% [41 of 48] vs. 41.7% [20 of 48], $P < 0.0001$) in the surveyed patients (Figure 2D). When both markers were combined, the responders were found to be 72.0% (18 of 25) in PD-L1^{hi}PVR^{lo}, 43.5% (10 of 23) in PD-L1^{lo}PVR^{lo}, 25.9% (7 of 27) in PD-L1^{hi}PVR^{hi}, and 0% (0 of 21) in PD-L1^{lo}PVR^{hi} (Figure 2, D and E). The response to PD-1 blockade in PD-L1^{hi} patients was significantly higher in low PVR expression than in high PVR expression (72.0% [18 of 25] vs. 25.9% [7 of 27], $P < 0.0001$). It is also worthwhile to note that high PVR expression in PD-L1^{lo} patients predicted nonresponders with very high accuracy compared with low PVR expression (100% [21 of 21] vs. 56.5% [13 of 23], $P = 0.001$). These data indicate that increased PVR expression in both PD-L1^{hi} patients and PD-L1^{lo} patients deteriorates the accuracy predicting the responders to anti–PD-1 or anti–PD-L1 therapy in NSCLC patients.

PD-L1^{hi} patients have been considered to show significantly longer progression-free survival (PFS) after PD-1 blockade than PD-L1^{lo} patients. Our PFS data for the 96 patients also confirmed this finding (i.e., 5.1 vs. 1.95 months, $P = 0.0008$; Figure 2F, top). Interestingly, the PVR^{hi} patients among the 96 patients showed a significantly shorter median PFS after PD-1 blockade than the PVR^{lo} patients (1.95 vs. 6.5 months, $P = 0.0005$; Figure 2F, middle). For the 4 groups, the median PFS values were found to be 1.4 months in PD-L1^{lo}PVR^{hi}, 2.8 months in PD-L1^{lo}PVR^{lo}, 13 months in PD-L1^{hi}PVR^{lo}, and 2.45 months in PD-L1^{hi}PVR^{hi} (Figure 2F, bottom). Compared with the survival patterns in Figure 1D, the PD-L1^{hi}PVR^{hi} and PD-L1^{hi}PVR^{lo} groups, which correspond to hi/lo and hi/hi groups in Figure 1D, were shifted toward good prognosis as a result of PD-1 blockade. Consistent with this finding, the PFS distribution of individual patients demonstrated that the PD-L1^{hi}PVR^{lo} group was enriched in patients with longer PFSs, while the PD-L1^{lo}PVR^{hi} group was enriched in patients with shorter PFSs (Supplemental Figure 2C). Collectively, these results indicated that the PFS difference between the PD-L1^{hi}PVR^{lo} and PD-L1^{lo}PVR^{hi} groups (PFS 13 vs. 1.4 months, $P < 0.0001$) was significantly increased compared with the difference between the PD-L1^{hi} and PD-L1^{lo} (5.1 vs. 1.95 months) or PVR^{hi} and PVR^{lo} (1.95 vs. 6.5 months) groups. Moreover, the PD-L1^{hi}PVR^{lo} group had a significantly longer PFS than the PD-L1^{hi}PVR^{hi} group (13 vs. 2.45 months, $P = 0.0276$). Similar trends were observed for overall survival (OS) (Supplemental Figure 2D). The PD-L1^{hi} patients among the 96 patients showed a significantly longer median OS after anti–PD-1 therapy than the PD-L1^{lo} patients (21.9 vs. 7.9 months, $P = 0.0699$; Supplemental Figure 2D, top). The PVR^{hi} patients showed a significantly shorter median OS after PD-1 blockade than the PVR^{lo} patients (7.6 vs. 14.2 months, $P = 0.032$; Supplemental Figure 2D, middle). For the 4 groups, the median OS values were 6.5 months for PD-L1^{lo}PVR^{hi}, 8.7 months for PD-L1^{lo}PVR^{lo}, 23.3 months for PD-L1^{hi}PVR^{lo}, and 9.7 months for PD-L1^{hi}PVR^{hi} (Supplemental Figure 2D, bottom).

Moreover, in Cox regression models adjusted for age, sex, smoking, histology, EGFR mutation, and treatment time, the adjusted hazard ratios (AHRs) for the risk of progression to PD-1 blockade were 2.194 (95% CI, 1.276–3.772; $P = 0.001$) for PVR^{hi} patients and 0.430 (95% CI, 0.262–0.706; $P = 0.001$) for PD-L1^{hi} patients, and 0.346 (95% CI, 0.183–0.654; $P = 0.001$) for PD-L1^{hi}PVR^{lo} patients (Table 2).

Table 1. Patient characteristics according to PD-L1/PVR expression in discovery set

Variables	No. of samples	PD-L1/PVR expression				P value
		lo/hi	lo/lo	hi/lo	hi/hi	
Age (year)						
<65	49 (51%)	12 (12.5%)	11 (11.5%)	8 (8.3%)	18 (18.8%)	0.0830
≥65	47 (49%)	9 (9.4%)	12 (12.5%)	17 (17.7%)	9 (9.4%)	
Sex						
Male	69 (71.9%)	13 (13.5%)	18 (18.8%)	20 (20.8%)	18 (18.8%)	0.4440
Female	27 (28.1%)	8 (8.3%)	5 (5.2%)	5 (5.2%)	9 (9.4%)	
Smoking status						
Never smoker	30 (31.2%)	7 (7.3%)	6 (6.2%)	7 (7.3%)	10 (10.4%)	0.8320
Ever smoker	66 (68.8%)	14 (14.6%)	17 (17.7%)	18 (18.8%)	17 (17.7%)	
Histology						
Adenocarcinoma	62 (64.6%)	15 (15.6%)	17 (17.7%)	10 (10.4%)	20 (20.8%)	0.0300
Squamous carcinoma	34 (35.4%)	6 (6.2%)	6 (6.2%)	15 (15.6%)	7 (7.3%)	
EGFR status						
WT	86 (89.6%)	19 (19.8%)	21 (21.9%)	24 (25.0%)	22 (22.9%)	0.3770
Mutant[A]	10 (10.4%)	2 (2.1%)	2 (2.1%)	1 (1.0%)	5 (5.2%)	
ALK status						
WT	95 (99.0%)	21 (21.9%)	23 (24.0%)	25 (26.0%)	26 (27.1%)	0.4610
Rearrangement	1 (1.0%)	0 (0%)	0 (0%)	0 (0%)	1 (1.0%)	
Immunotherapeutic agent						
Nivolumab	67 (69.8%)	16 (16.7%)	20 (20.8%)	12 (12.5%)	19 (19.8%)	0.0670
Pembrolizumab	26 (27.1%)	3 (3.1%)	2 (2.1%)	13 (13.5%)	8 (8.3%)	
Atezolizumab	3 (3.1%)	2 (2.1%)	1 (1.0%)	0 (0%)	0 (0%)	
Response to PD-1 blockade						
Responder[B]	35 (36.5%)	0 (0%)	10 (10.4%)	18 (18.8%)	7 (7.3%)	0.0001
Nonresponder	61 (63.5%)	21 (21.9%)	13 (13.5%)	7 (7.3%)	20 (20.8%)	

[A]EGFR mutant type, Exon19deletion (n = 5), Exon19deletion/T790M (n = 1), Exon 21 L858R (n = 4), and Exon18 S768I (n = 1). [B]Responder, the patients who show partial response or stable disease (≥6 months)

To confirm these findings, we established the independent validation set composed with 94 NSCLC patients treated with anti–PD-1 or anti–PD-L1 therapy. Baseline characteristics of the discovery cohort and the validation cohort were similar (Supplemental Table 1). The response rate to PD-1 blockade was 39% in the discovery cohort (Supplemental Figure 3A). Based on the same cutoff used in the discovery set, the patients were distributed into PD-L1^{lo}PVR^{hi} (14 of 94, 16%), PD-L1^{lo}PVR^{lo} (38 of 94, 41%), PD-L1^{hi}PVR^{lo} (20 of 94, 21%), and PD-L1^{hi}PVR^{hi} (22 of 94, 22%) (Supplemental Table 2). Consistent with those in the discovery set, the PD-L1^{hi} group and PVR^{hi} group enriched responders and nonresponders, respectively, in the validation set (Supplemental Figure 3B), and the responders to PD-1 blockade were also the mostly enriched in PD-L1^{hi}PVR^{lo} (70%) among all the groups (Supplemental Figure 3C). Moreover, the PFS of the PD-L1^{hi}PVR^{lo} group was much longer than those in others, but that of PD-L1^{lo}PVR^{hi} group was the shortest (10.7 months in PD-L1^{hi}PVR^{lo}, 3.0 months in PD-L1^{lo}PVR^{lo}, 4.8 months in PD-L1^{hi}PVR^{hi}, and 1.7 months in PD-L1^{lo}PVR^{hi}) (Supplemental Figure 3D). Similarly to the discovery set, the Cox regression model consistently showed the 0.370 as AHRs (95% CI, 0.182–0.755; P = 0.006) for the risk of progression to PD-1 blockade for PD-L1^{hi}PVR^{lo} patients (Supplemental Table 3).

Taken together, these data in the discovery as well as validation sets suggest that the accuracy in predicting treatment outcomes including objective response rate (ORR) and PFS after PD-1 blockade can be improved when both PD-L1 and PVR expression levels are considered.

PD-L1 and PVR promote tumor growth by differentially modulating tumor-infiltrating immune cells. To understand the functional implications of PVR and its functional association with PD-L1, we first investigated tumor growth and survival in PD-L1–KO or/and PVR-KO tumor-bearing mice. MC38 mouse tumor cells express both PD-L1 and PVR and are responsive to PD-1 blockade. Using these cells and the CRISPR/Cas9 system, we established 4 tumor cell types that express PD-L1 and PVR differently (Figure 3A): (a) PD-L1^{+}PVR^{+} (WT); (b) PD-L1^{-}PVR^{+} (PD-L1–KO); (c) PD-L1^{+}PVR^{-} (PVR-KO); (d) PD-L1^{-}PVR^{-} cells (PD-L1/PVR–double KO;

Table 2. Univariate and multivariate factors affecting the response to anti–PD-1 therapy

Variable	Category	Univariate survival analysis			Multivariate survival analysis		
		HR	95% CI	*P* value	AHR	95% CI	*P* value
Age (years)	≥65 vs. <65	0.773	0.489–1.221	0.270	0.969	0.595–1.580	0.901
Sex	Female vs. male	2.200	1.339–3.617	0.002	1.881	0.675–5.236	0.227
Smoking	Smoker vs. never smoker	0.548	0.340–0.884	0.014	0.779	0.282–2.151	0.630
Histology	Squamous vs. nonsquamous	0.827	0.509–1.345	0.445	1.787	0.987–3.235	0.055
EGFR status	Mutant vs. WT	1.960	0.965–3.979	0.063	1.522	0.700–3.310	0.289
Treatment line	≥ 3rd line vs. 2nd line	1.260	0.796–1.994	0.323	1.161	0.702–1.921	0.561
PD-L1[A]	≥10% vs. <10%	0.458	0.289–0.727	0.001	0.420	0.254–0.696	0.001
PVR[A]	≥60% vs. <60%	2.001	1.262–3.175	0.003	2.303	1.344–3.947	0.002
PD-L1/PVR status[A]	PD-L1$^+$/PVR$^-$ vs. others	0.406	0.229–0.718	0.002	0.337	0.180–0.634	0.001

HR, hazard ratio; AHR, adjusted hazard ratio; CI, confidence interval. [A]In multivariate analysis, 1 factor of PD-L1, PVR, and PD-L1/PVR is included for analysis.

dKO) (Figure 3A). As previously reported, after IFN-γ treatment, PD-L1 was upregulated in WT and PVR-KO cells, but not in PD-L1–KO and –dKO cells, while PVR expression was not changed in all types of cells (Supplemental Figure 4). After injecting each tumor cell type into the mice, the tumor growth and survival in the tumor-bearing mice was monitored over time (Figure 3, B and C). PD-L1 and PVR-KO WT tumors reached a size above 2000 mm^3. Two and 1 out of 8 PD-L1 and 8 PVR-KO tumors, respectively, were rejected. Notably, in dKO tumors, tumor growth was delayed more significantly than in PD-L1–KO or PVR-KO tumors, and half (4 of 8) were tumor free (Figure 3B). A similar trend was observed in the survival of mice bearing the 4 tumor cell types (Figure 3C), consistent with the survival patterns in Figure 1D, where WT and dKO tumors, which correspond to the hi/hi and lo/lo groups in Figure 1D, showed the worst and best survival rates, respectively. Collectively, these data suggest that PD-L1 or PVR expression promotes tumor progression and has a synergistic effect on tumor growth, possibly via independent immunosuppressive mechanisms.

Despite the controversy regarding whether PD-L1 for tumor-immune evasion originates from tumor or host cells in tumor-bearing mice, PD-L1 from MC38 tumor cells was recently reported to be sufficient for the suppression of the antitumor immunity of T cells (24–26). Our study also showed retarded growth of PD-L1–KO tumor compared with WT tumor, even though PD-L1 expressions on CD45.2$^+$ tumor-infiltrating immune cells were similar between WT tumor and PD-L1–KO tumor (Supplemental Figure 5). Meanwhile, PVR expression on CD45.2$^+$ tumor-infiltrating immune cells was decreased when tumor cells were deprived of PVR (Supplemental Figure 5). This result suggests that PVR expression on tumor cells is more critical to tumor-immune escape and tumor progression than that on tumor-infiltration leukocytes. However, since PD-L1 maintains its expression level on tumor-infiltrating immune cells even without tumor PD-L1 expression, it cannot be ruled out that PD-1 blockade might still contribute to the functional restoration of exhausted T cells by inhibiting the ligation of PD-L1 expressed by tumor-infiltrating immune cells. Thus, we focused on determining which cellular source of PVR was critical for tumor-immune evasion by analyzing the tumor growth and survival of the aforementioned 4 MC38 tumor cell types in PVR and PD-L1–KO mice. Superior tumor growth control and survival rates were observed in tumor cells compared with host cells when PVR or PD-L1 was absent (Supplemental Figure 6), suggesting that tumor-expressing PVR or PD-L1 is more critical to tumor-immune escape and tumor progression.

Next, we sought to elucidate PD-L1– or PVR-mediated alterations in tumor-infiltrating immune cells. After injecting WT, PD-L1–KO, or PVR-KO MC38 tumor cells into mice, we compared the infiltration and function of T cells in tumors once the tumors had been stably established in vivo. Interestingly, PVR KO more significantly enhanced CD8$^+$ T cell infiltration than PD-L1 KO (Figure 3, D and E). In contrast, PD-L1 KO significantly enhanced CD4$^+$ T cell infiltration, but PVR KO was comparable with WT in terms of CD4$^+$ T cell infiltration (Figure 3, D and F). Among tumor-infiltrating CD4$^+$ T cells, the majority were immune-suppressive Foxp3$^+$ Tregs (Figure 3, G and H). PVR KO significantly reduced the infiltration of these Tregs, compared with WT or PD-L1 KO, resulting in a high CD8$^+$ T cell/Treg ratio (Figure 3, G–I). CD8$^+$ T cells have been previously demonstrated to be critical immune killer cells that exert antitumor immunity under the control of immune checkpoint pathways (15, 26). We thus examined whether PD-L1 or PVR KO affected the function of CD8$^+$ tumor-infiltrating lymphocytes (TILs). PD-L1

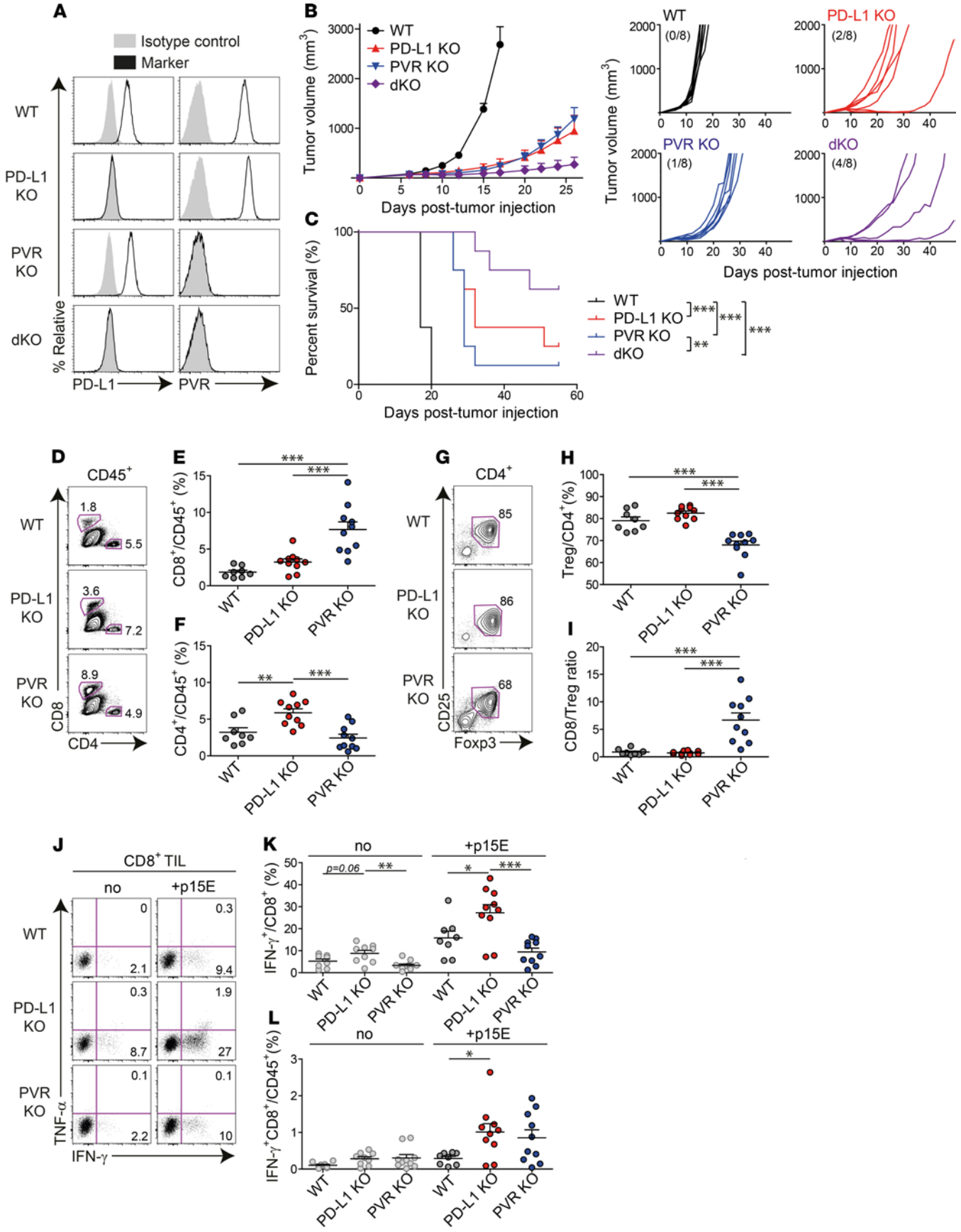
A
Isotype control
Marker
WT
PD-L1 KO
PVR KO
dKO
% Relative
PD-L1
PVR
B
WT
PD-L1 KO
PVR KO
dKO
Tumor volume (mm3)
Days post-tumor injection
WT (0/8)
PD-L1 KO (2/8)
PVR KO (1/8)
dKO (4/8)
C
Percent survival (%)
Days post-tumor injection
***
**
D
CD45+
CD8
CD4
E
CD8+/CD45+ (%)
F
CD4+/CD45+ (%)
G
CD4+
CD25
Foxp3
H
Treg/CD4+ (%)
I
CD8/Treg ratio
J
CD8+ TIL
no
+p15E
TNF-α
IFN-γ
K
IFN-γ+/CD8+ (%)
p=0.06
L
IFN-γ+CD8+/CD45+(%)

Figure 3. PD-L1 and PVR promote tumor growth by differentially modulating tumor-infiltrating immune cells. (**A**) PD-L1– or/and PVR-deficient MC38 tumor cells were generated from parental WT MC38 and expression of PD-L1 and PVR was assessed by flow cytometry. (**B** and **C**) B6 mice were injected s.c. with WT (black), PD-L1–KO (red), PVR-KO (blue), or dKO (purple) MC38 tumor cells (1×10^5 cells each, $n = 8$ per group). Tumor growth (**B**) and survival (**C**) of each tumor-bearing mouse. Numbers in parentheses denote the tumor-free mice/total mice on day 49 after transplantation. The data are represented as the mean ± SEM and are representative of 2 independent experiments. $^{**}P < 0.01$ and $^{***}P < 0.001$ by multivariate Wilcoxon with multiple comparison test. (**D–H**) Once established (100–200 mm^3), each tumor harvested from WT (black, $n = 8$), PD-L1–KO (red, $n = 10$), or PVR-KO (blue, $n = 10$) MC38-bearing mice was analyzed by flow cytometry. Representative FACS plots (**D**) and frequency of $CD8^+$ T cells (**E**) or $CD4^+$ T cells (**F**) among $CD45^+$ cells in tumors. Representative FACS plots (**G**) and frequency of $CD4^+Foxp3^+CD25^{hi}$ Tregs (**H**) among $CD45^+CD4^+$ T cells. (**I**) The ratio of $CD8^+$ T cells/Tregs in harvested tumors. (**J–L**) $CD8^+$ T cells in each harvested tumor were ex vivo stimulated with or without MC38 epitope peptide (p15E, KSPWFTTL). Representative FACS plots (**J**) and frequency of IFN-γ^+ cells among $CD8^+$ T cells (**K**) and IFN-γ^+ $CD8^+$ T cells (**L**) in each tumor type. The data are represented as the mean ± SEM with each dot indicating 1 mouse. $^{*}P < 0.05$; $^{**}P < 0.01$; and $^{***}P < 0.001$ by 1-way ANOVA with Tukey's multiple comparison test.

KO enhanced the IFN-γ–producing capability of tumor-specific $CD8^+$ TILs, while PVR KO showed no significant enhancement in response to stimulation of p15E peptide, an MHC class I–restricted epitope of MC38, compared with WT. However, PVR KO showed a comparable effect in terms of the infiltration of IFN-γ–producing $CD8^+$ TILs to PD-L1 KO due to enhanced $CD8^+$ TIL infiltration (Figure 3, J–L). Recently, TIGIT-expressing NK cells were reported to play important roles in tumor control (27). Thus, we investigated the infiltration and function of NK cells in tumors. Similar to the observations for $CD8^+$ T cells, PVR KO significantly enhanced NK cell infiltration compared with PD-L1 KO, while PD-L1 KO enhanced the IFN-γ production of NK cells (Supplemental Figure 7). These data suggest that PD-L1 and PVR differentially modulate the infiltration and function of TILs.

Differential sensitivity for checkpoint blockade therapy depending on the expression pattern of checkpoint ligand PD-L1 and PVR. As described above, we demonstrated that the responders to PD-1 blockade were enriched in $PD\text{-}L1^{hi}PVR^{lo}$ patients, while the nonresponders were enriched in $PD\text{-}L1^{lo}PVR^{hi}$ patients. Thus, next, we sought to validate the effect of PD-L1 and PVR expression on the responsiveness to anti–PD-1 therapy using the aforementioned MC38 tumor–bearing mice. After injecting WT, PD-L1–KO, or PVR–KO MC38 cells into mice, we treated the tumor-bearing mice with anti–PD-1 or isotype control. Then, we analyzed the tumor growth and survival of the tumor-bearing mice. Anti–PD-1 treatment significantly delayed tumor growth and improved survival in WT and PVR-KO tumor-bearing mice, compared with isotype control treatment, but showed marginal effects in PD-L1–KO tumor-bearing mice (Figure 4, A–F). Moreover, compared with WT, PVR KO further significantly delayed tumor growth and survival after anti–PD-1 treatment (Figure 4, A, B, E, and F). To confirm the differential efficacy of PD-1 blockade between PD-L1–KO tumor and PVR-KO tumor, CT26 tumor cells, which were known to be less sensitive to anti–PD-1 therapy, were also genetically engineered not to express PD-L1 or PVR (Supplemental Figure 8A). Similar to MC38 tumors, PD-L1–KO and PVR-KO CT26 tumors showed a delayed growth in vivo compared with WT CT26 tumors (Supplemental Figure 8B). More importantly, PVR-KO CT26 tumors seemed to be responsive to anti–PD-1 therapy, while PD-L1–KO CT26 tumors were resistant (Supplemental Figure 8C). Consistent with our previous findings from 2 different cohorts of NSCLC patients (Figure 2F and Supplemental Figure 3D), these data suggest that PVR expression reduces the responsiveness to anti–PD-1 therapy, as opposed to PD-L1, whose expression enhances responsiveness.

PD-L1–KO tumor-bearing mice were marginally responsive to anti–PD-1 therapy. Therefore, we next investigated whether PVR-TIGIT blockade by anti-TIGIT therapy could affect tumor growth and survival in a complementary manner to PD-1 blockade. After injecting PD-L1–KO MC38 cells into mice, we treated the tumor-bearing mice with isotype control, anti-TIGIT, or a combination of anti-TIGIT and anti–PD-1 (anti-TIGIT + anti–PD-1) therapies and then compared the resulting tumor growth and survival. Intriguingly, although PD-L1–KO tumor-bearing mice were insensitive to anti–PD-1 therapy, anti-TIGIT treatment delayed tumor growth in these mice, and anti-TIGIT + anti–PD-1 delayed tumor growth more significantly (Figure 4G). The same trend was observed regarding survival (Figure 4H). Moreover, more mice were found to be tumor free when treated with anti-TIGIT or anti-TIGIT + anti–PD-1 compared with when treated with the isotype control (anti-TIGIT, 3 of 10; anti-TIGIT + anti–PD-1, 4 of 10; and isotype control, 1 of 10). In PD-L1–KO tumor-bearing mice, the tumor-infiltrating immune cells still expressed high levels of PD-L1 in the host (Supplemental Figure 5), which could explain the superior effect of anti-TIGIT + anti–PD-1 compared with anti-TIGIT alone (Figure 4, G and H).

In conclusion, we demonstrate that ICL pairing can provide a better understanding of responsiveness to ICB therapy, and we allow for the stratification of cancer patients based on the expression of the ICL pair to the clinical outcomes of therapy.

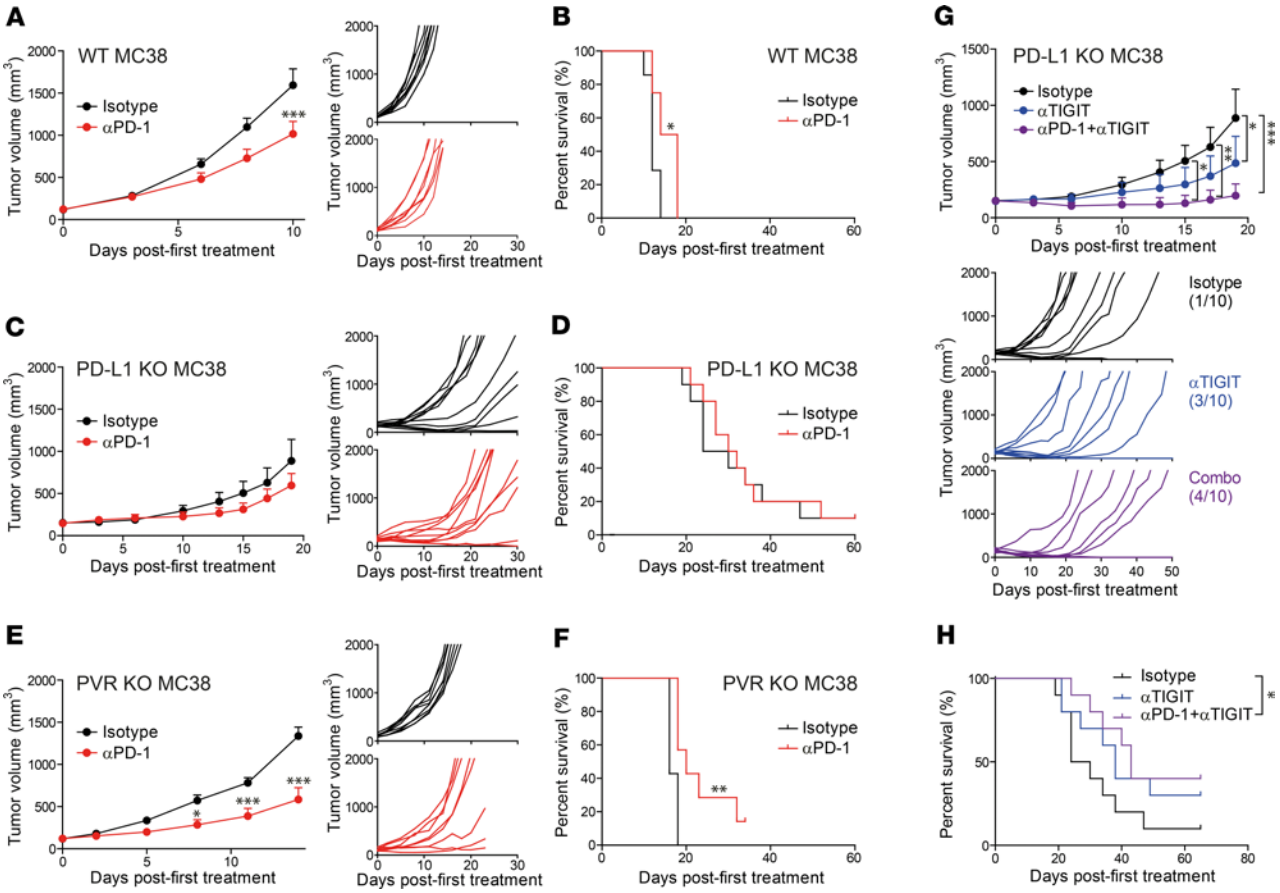

Figure 4. Differential sensitivity for checkpoint blockade therapy depending on the expression pattern of checkpoint ligand PD-L1 and PVR. B6 mice were injected s.c. with WT (n = 8), PD-L1–KO (n = 10), or PVR-KO (n = 8) MC38 tumor cells and treated i.p. with 200 μg of isotype control (black), anti–PD-1 (red), anti-TIGIT (blue), or anti–PD-1 + anti-TIGIT (violet, each 200 μg) per time (total 5 times, every 3 days), once each tumor was established (100–200 mm^3). (**A**–**F**) Tumor growth (**A**, **C**, **E**) and survival (**B**, **D**, **F**) of WT MC38- (**A** and **B**), PD-L1–KO MC38- (**C** and **D**), or PVR-KO MC38-bearing (**E** and **F**) mice after anti–PD-1 therapy. The data are represented as the mean ± SEM and are representative of 3 independent experiments. (**G** and **H**) Tumor growth (**G**) and survival (**H**) of PD-L1–KO MC38-bearing mice (n = 10) after treatment with anti-TIGIT alone (blue) or with anti–PD-1 (purple). The numbers in parentheses show the tumor-free mice/total mice on day 60 after transplantation. The data are represented as the mean ± SEM and are representative of 2 independent experiments. $^*P < 0.05$; $^{**}P < 0.01$; and $^{***}P < 0.001$ by 2-way ANOVA with multiple comparison test (**A**, **C**, **E**, **G**), Wilcoxon test(**B**, **D**, **F**), or multivariate Wilcoxon with multiple comparison test (**H**).

Discussion

In this study, we explored the expression profiles of ICLs in different types of cancers and provided a framework for the identification of a potential ICL-based biomarker for the blockade of PD-1 and other ICRs. Among many ICLs, PVR was found to be independently expressed with PD-L1 in public RNA-seq data and NSCLC patients. As an independent parameter distinct from PD-L1, high PVR expression strongly enriched nonresponders for PD-1 blockade in NSCLC patients of both discovery and validation cohorts, resulting in a greater enrichment of responders in PD-$L1^{hi}PVR^{lo}$ patients and nonresponders in PD-$L1^{hi}PVR^{hi}$ or PD-$L1^{lo}PVR^{hi}$ patients. Indeed, in a mouse tumor model, the deletion of PVR enhanced the sensitivity to anti–PD-1 therapy, and the deletion of PD-L1 reduced this sensitivity. PD-L1–KO tumors were insensitive to anti–PD-1 but responsive to anti-TIGIT, and even more so to anti-TIGIT combined with anti–PD-1. Our data suggest that the sensitivity of checkpoint blockade therapy could depend on the expression pattern of checkpoint ligands.

We investigated the reasons for high PVR expression in strongly enriched nonresponders for PD-1 blockade in NSCLC patients and found a strong involvement of the PVR/TIGIT pathway with tumor progression in NSCLC patients. Consistent with previous reports (27, 28), PVR was highly expressed in the tumor tissues of NSCLC patients, as the median cutoff value of TPS reached ~60% compared with that of PD-L1, at ~10%. Its paired inhibitory receptor TIGIT is also reported to be highly expressed in tumor-infiltrating T cells in NSCLC patients (15, 29). However, another paired stimulatory receptor,

CD226, may not be ligated well to PVR because of the higher affinity of TIGIT to PVR than CD226 and in cis disruption of CD226 by TIGIT in the TME (11, 15). This may lead to PVR transducing inhibitory signals in the same manner as PD-L1 in tumors. Moreover, PVR was found to be a strong prognostic factor for patient survival in LUAD of TCGA ($P = 0.0005$). Our results do not rule out that the superior responsiveness of PVR^{lo} patients is due to the prognostic power of PVR; however, our mouse data experimentally demonstrate that the genetic absence of PVR could enhance tumor sensitivity to PD-1 blockade.

The roles of tumor PD-L1 and host PD-L1 in cancer are yet to be fully elucidated. According to the current literature, tumor PD-L1 suppresses tumor control via the immune system, and host PD-L1 is dependent on conditions such as the immunogenicity of tumor cells (24–26, 30). In our tumor model, tumor PD-L1 or PVR showed much stronger tumor suppression than host PD-L1 or PVR in controlling tumor growth and survival (Supplemental Figure 6). This may be because immune cells express molecules that transduce both costimulatory and coinhibitory signals to T cells, while tumor cells express coinhibitory molecules but rarely express costimulatory molecules (31). However, when tumor ligation of the inhibitory signal is absent, immune cells seem to be more flexible to environmental changes than tumor cells. Deletion of tumor PD-L1 induced the upregulation of PD-L1 in host myeloid cells as a resistance mechanism (24). This may explain why the combination of anti-TIGIT and anti–PD-1 therapies was more effective than anti-TIGIT treatment alone in PD-L1–KO tumor bearing mice.

Compared with the ICR studies using KO mice, functional studies of ligand ICLs in TMEs are only just starting to be explored, owing to the development of CRISPR/Cas9 technology. The role of tumor PD-L1 on tumor control by $CD8^+$ T cells and NK cells has been proven in recent studies, where PD-L1 on tumor cells were found to protect them from direct killing via a slight increase of the T cell population (24–26, 30). In our study, PD-L1 on tumor cells was found to restrict the function of tumor-reactive $CD8^+$ T cells in vivo; PD-1 seems to regulate signal 3 of T cells, as well as a previously identified costimulatory signal, signal 2, of T cells (32, 33). Moreover, consistent with a very recent report (30), NK cells also produced more effector cytokines in the absence of tumor PD-L1. On the other hand, tumor PVR regulated a different aspect of T cells/NK cells. Consistent with another recent report (34), PVR KO in tumors enhanced tumor control (Figure 3B and Supplemental Figure 8B) and sensitivity to PD-1 blockade (Figure 4, E and F; and Supplemental Figure 8C). In our study, we suggest that PVR expression in tumors seems to affect antitumor immune response in 2 different ways, which might give rise to increased sensitivity to PD-1 blockade. First, PVR-KO tumor-infiltrating immune cells, especially Tregs, expressed PD-1 more frequently than do WT or PD-L1–KO tumor-infiltrating immune cells (Supplemental Figure 9). Second, interestingly, the absence of tumor PVR significantly increased $CD8^+$ T cells and NK cells but reduced Tregs in tumors (Figure 3, E–L, and Supplemental Figure 7). This might be attributed to changes in apoptosis, proliferation, or migration of $CD8^+$ T cells, NK cells, and Tregs. $TIGIT^+CD8^+$ T cells were shown to be more apoptotic than $TIGIT^-CD8^+$ T cells isolated from the PBMC of acute myeloid leukemia (AML) or gastric cancer patients (35, 36). The blockade of TIGIT was found to enhance the proliferation of $CD8^+$ T cells from melanoma patients in another study (13). TIGIT signaling has also been implicated in promoting Treg migration and retention in tumor tissues (37). Together, these distinct mechanisms regulated by PD-L1 and PVR may explain the synergy in tumor control by PD-1 and TIGIT/CD96 blockade (34).

Considering PD-L1 and PVR expressions in tumor cells or tumor-infiltrating immune cells, the expression of PVR — but not that of PD-L1 — was more dominant in tumor cells than in immune cells of the host (Supplemental Figure 5), suggesting the importance of tumor PVR expression as a mechanism of immune evasion in TME. Meanwhile, there was a report showing that PVR-KO tumor was still responsive to TIGIT/CD96 blockade (34), which implies the role of PVR expression in host immune cells. This finding prompted us to examine the expressions of TIGIT/CD96 and PVR on immune cells in the TME. Interestingly, both TIGIT and CD96 have been upregulated on immune cells in PVR-KO tumors compared with those in WT tumors (Supplemental Figure 10). In contrast, PVR has been rather downregulated on immune cells in PVR tumors compared with WT tumors (Supplemental Figure 5). Therefore, it is necessary to further investigate which cell type expressing PVR can play a more important role in immune suppressive mechanism under TME and whether additional TIGIT/CD96 blockade is still required even when tumor cells are deficient in PVR expression.

Several early-phase clinical trials using anti-TIGIT therapy either alone or in combination with PD-1 blockade are currently being conducted in nonselected solid cancer populations, including NSCLC (38). One recent study demonstrated 3% ORR and 35% disease control rate (DCR) for anti-TIGIT alone and 19% ORR and 47% DCR for anti-TIGIT + anti–PD-1 in heavily treated solid cancer patients. This result paradoxically suggests that patient selection using a stratified biomarker is means by which to enrich the response to immunotherapy.

Despite having improved patient stratification PD-L1 and PVR, the prediction is still not fully complete as 100%. This indicates that there are still multiple pathways other than PD-L1/PD-1 or PVR/TIGIT that inhibit antitumor immunity or promote tumor progression, leading to the resistance for PD-1 blockade. In our ICL expression correlation data (Figure 1A), *CEACAM1*, *CD276*, or *VTCN1*, as well as *PVR*, are independently expressed with PD-L1, suggesting that these could also be potential biomarker candidates for anti–PD-1. Recently, despite involving a limited number of patients, one study found that CD276 with PD-L1 expression was a potential biomarker for anti–PD-1 (39). Eventually, to achieve a higher responder rate, further ICL-based biomarkers and a patient-specific set of verified ICLs would enrich responders for anti–PD-1. Moreover, multiple immunosuppressive cells, such as myeloid-derived suppressor cells (MDSCs), TGF-β, or low tumor mutational burden (TMB), in other types of cancer have been reported to result in resistance to anti–PD-1 therapy (40–44). Finally, it would be interesting to study the relationship among these cells and consolidate the parameters to obtain a biomarker for precision medicine. Consequently, our data clinically and experimentally demonstrate that patient-specific expression of selected ICLs can enrich responders or nonresponders for ICR blockade therapy to achieve a superior selection of patients for personalized therapy.

Methods

Study design and clinical efficacy analysis. This study was conducted in a cohort of histologically confirmed stage IV NSCLC patients treated with anti–PD-1 therapy (nivolumab 2 mg/kg every 2 weeks, pembrolizumab 200 mg fixed dose every 3 weeks, or atezolizumab 1200 mg fixed dose every 3 weeks) at Yonsei Cancer Center between 2013 January and 2018 February. The criteria used for patient selection included the availability of (a) tumor tissue, (b) smoking history, (c) genetic data (EGFR and ALK mutant), (d) treatment outcome to anti–PD-1 therapy, and (e) survival data. A total of 96 consecutive NSCLC patients treated with anti–PD-1 therapy were enrolled in this study.

A predesigned data collection format was used to review the patients' medical records for the evaluation of clinicopathological characteristics and treatment outcomes. Clinical responses were classified using the Response Evaluation Criteria in Solid Tumor (RECIST version 1.1). Treatment outcomes of this study were categorized into 2 groups (responders and nonresponders). Responder (R) was defined as PR or SD lasting longer than 6 months, whereas nonresponder (NR) was defined as progression of disease ≤ 6 months of initiating anti–PD-1 therapy. PFS was measured from the first day of anti–PD-1 therapy to tumor progression or death, while OS was measured from the date of anti–PD-1 therapy until the date of death. We assessed whether each subset by PD-L1 and PVR affected treatment outcome (R/NR, PFS, or OS) in this study. Patients were censored on June 5, 2018, if alive and progression free. Patients without a known date of death were censored at the time of last follow-up.

Correlation analysis of ICL and ICR gene expression levels. For the correlation analysis of ICLs and ICRs, we collected 4 microarray data sets from the gene expression omnibus database (GSE10245, GSE30219, GSE31210, and GSE37745; https://www.ncbi.nlm.nih.gov/geo) and an RNA-seq data set from TCGA database (TCGA-LUAD; https://portal.gdc.cancer.gov) (17–20). For each microarray data set, we normalized the $\log_2$ intensities using the quantile normalization method (45) and then used the normalized intensities for analysis. For the analysis of the RNA-seq data set, the normalized fragments per kilobase of transcript per million mapped reads (FPKM) values from the TCGA database were used. For the integrative correlation analysis, we first calculated Spearman's correlations (46) for all pairs of 27 ICLs in each of the 5 data sets. For each pair of ICLs, we then combined the Spearman's correlations from the 5 data sets into a representative correlation as the weighted mean of the 5 correlations by the sample sizes of the corresponding data sets, based on Schmidt–Hunter method, a well-known meta-analysis method (22). To identify clusters of ICLs with strong coexpression patterns, we next applied a hierarchical clustering (Euclidean distance as a dissimilarity measure and single linkage method) to the representative correlations for all the pairs of the 27 ICLs. Among the resulting clusters, we finally selected 2 clusters showing virtually no correlations between them.

Survival analysis. We chose to use the 2 data sets (TCGA and GSE31210), with more than 200 patients, for survival analysis to ensure a sufficient sample size (≥30 samples/group) in each of the 4 groups shown in Figure 1D (hi/hi, hi/lo, lo/hi, and lo/lo). For each ICL, the patients in the 2 cohorts were divided into 2 groups with high (≥ 50th percentile, hi) and low (≤ 50th percentile, lo) expression of the target gene (e.g., PVR). The cumulative event (death) rate was calculated for each patient group using the Kaplan–Meier method (47). The survival curves of the 4 patient groups were compared using the multivariate Wilcoxon with multiple comparison test.

PD-L1 and PVR IHC and scoring. Formalin-fixed, paraffin-embedded (FFPE) tissues were sectioned at a thickness of 4 μm and stained using Ventana BenchMark XT automated staining platform (Ventana Medical Systems). For the PD-L1 IHC assay, the sections were stained with an anti–PD-L1 (clone SP263, Ventana Medical Systems) rabbit monoclonal primary antibody using the OptiView DAB IHC Detection kit as previously reported (48). For PVR IHC assay, PVR antibody (rabbit monoclonal, clone D8A5G, Cell Signaling Technology) was diluted to 1:100, treated, and incubated at 37°C for 32 minutes. Signals were detected using ultraview universal DAB Detection Kit (Ventana Medical Systems). The PD-L1 and PVR scores in tumor cells were interpreted as the tumor proportion score (TPS) according to the methods of previous studies (49). TPS was defined as the percentage of partial or complete stained viable tumor cells with any intensities in a section that included at least 100 tumor cells.

Cell culture and gene deletion using CRISPR/Cas9 system. MC38 were a gift from Seung-woo Lee's laboratory (POSTECH) and cultured in DMEM (Corning) supplemented with 10% FBS (Thermo Fisher Scientific) and 1% penicillin/streptomycin (Thermo Fisher Scientific). MC38 cells were tested negative for mycoplasma contamination. To generate PD-L1–KO and/or PVR-KO MC38, MC38 cells were transiently transfected with PX459 plasmid (Addgene) expressing Cas9 and optimized sgRNA, targeting PD-L1 (PD-L1 sgRNA sequence, 5′-GTATGGCAGCAACGTCACGA-3′) or PVR (PVR sgRNA sequence, 5′-CTACAATTCGACAGGCGTCT-3′) (GenScript). After transfection and transient selection with puromycin (Invitrogen), cells were single-cell seeded into 96-well plates without puromycin. To select KO clones, the expression of PD-L1 and PVR was determined by flow cytometry, and the absence of PD-L1 was confirmed by treatment with IFN-γ (10 ng/mL) for 24 hours. PD-L1–KO and/or PVR-KO CT26 cells were also generated in the same way as described above.

Mouse tumor models. PD-L1–KO mice were originally generated by Lieping Chen (50). PVR-KO mice were purchased from Jackson Laboratory (catalog 020633). To obtain the tumor models, 1×10^5 WT, PD-L1–KO, PVR-KO, or PD-L1–PVR–dKO, MC38 cells in PBS and Matrigel (Corning) were injected s.c. into age-matched 6- to 8-week-old female C57BL/6 mice purchased from Orient Bio. Tumor sizes were measured using a caliper and calculated using the following formula at indicated time points: $1/2 \times (\text{length} \times \text{width}^2)$. Tumors larger than 2000 mm^3 were considered to be progressed, at which point the mice were killed. Mice with ulcerated tumors before progression were removed from study. In case of CT26 tumor model, 1×10^6 PD-L1–KO or PVR-KO CT26 cells in PBS were injected s.c. into age-matched 6- to 8-week-old female BALB/c mice purchased from Young Bio Inc. Tumor growth kinetics were monitored as above. All mice were maintained in a specific pathogen–free facility at Yonsei University.

Tissue harvest and flow cytometry. Upon collection, 100–200 mm^3 tumors were dissected and minced into small pieces (~1 mm) before digestion with 1 mg/mL collagenase type VI (Worthington Biochemical Corporation) for 20 minutes at 37°C to obtain single-cell suspensions. Single-cell suspensions of splenocytes were prepared by gentle mechanical disruption, followed by lysis with ACK lysis buffer to remove RBCs. For flow cytometric analysis of lymphocytes, single-cell suspensions were stained with the following antibodies: fluorochrome-conjugated antibodies against CD4 (clone RM4-5), CD8 (clone 53–6.7), CD45.2 (clone 104), CD25 (clone PC61), CD49b (clone DX5), PD-1 (clone 29F.1A12), TIGIT (clone 1G9), and PD-L1 (clone 10F.9G2) were from BioLegend; antibodies against PVR (clone 3F1), CD96 (clone 6A6), NK1.1 (clone PK136), and IFN-γ (clone XMG1.2) were from BD Biosciences; and antibodies against Foxp3 (clone FJK-16s) and TNF-α (clone MP6-XT22) were from Invitrogen. Dead cells were excluded by using LIVE/DEAD Fixable Violet Dead Cell Stain (Invitrogen). For Foxp3 staining, the cells were stained for surface antigens, followed by permeabilization, fixation, and staining using the Foxp3 Permeabilization/Fixation Kit and Protocol (Invitrogen). Intracellular cytokine staining of IFN-γ and TNF-α was performed using the Cytofix/Cytoperm Kit (BD Biosciences) according to the manufacturer's instruction. Flow cytometric data were collected on a FACSCantoII (BD) or CytoFLEX LX (Beckman Coulter) and analyzed using FlowJo software (Tree Star Inc.).

In vivo treatments. Mice were randomly divided into different treatment groups when tumor size reached 100–200 mm^3 (MC38) or 80–120 mm^3 (CT26). Mice were stratified based on the size of implanted tumor to ensure that tumor sizes were roughly equivalent between groups before the therapy. Each mouse was treated i.p. with 200 μg of isotype control, anti–PD-1 (RMP1-14, Bio X Cell), anti-TIGIT (1G9, Bio X Cell), or anti–PD-1 + anti-TIGIT (200 μg each) per time (total 5 times every 3 days).

Data and materials availability. All data associated with this study are present in the paper.

Statistics. Significant differences in variables according to each subset were tested using the χ^2 test, the Fisher's exact test, 1-way ANOVA, or 2-way ANOVA, as appropriate. The Kaplan–Meier method

was used to estimate PFS and OS, and the differences between subtypes were compared using the Gehan-Breslow-Wilcoxon test. AHRs for the risk of progression or death in response to anti–PD-1 therapy according to PD-L1/PVR status were calculated using a Cox regression model that included age, sex, smoking, histology, and genetic alterations as independent variables. All *P* values were based on a 2-tailed hypothesis. A *P* value less than 0.05 was considered significant.

Study approval. This study was approved by the IRB of Severance Hospital. All patients signed a written informed consent for genetic analysis (permit no. 4-20181161). All the animal experiments were conducted in accordance with the Korean Food and Drug Administration guidelines. Protocols were reviewed and approved by the IACUC of Yonsei University (permit no. IACUC-P-201810-01).

Author contributions

BRL, SC, and JM designed, performed, analyzed, and interpreted experiments and wrote the manuscript. SC performed bioinformatic analyses. HRK analyzed clinical data. BRL and JM performed the generation of KO tumor cell lines and in vivo mouse experiments. MJK helped analysis of FACS data. BCC provided patient material. HL, HWK, and HSS provided assistance with IHC. BCC, HSS, and HRK collected clinical data and participant samples. SJH, HRK, and DH supervised the project, designed and interpreted experiments, and wrote the manuscript.

Acknowledgments

We wish to thank S.W. Lee at POSTECH for providing MC38 cell line. We also thank I. Choi at Inje University for providing PD-L1–KO mice. We thank E.C. Shin and S.H. Park at KAIST for helpful discussion and useful comments with overall formatting of manuscript. We thank Flow Cytometry Core for help with establishing engineered cancer cell lines. This study was supported by the National Research Foundation of Korea (NRF) grant funded by the Korea government (MSIT) (2018R1A2A1A05076997 and 2017R1A5A1014560 to SJH; 2017R1D1A1B03029874, 2019M3A9B6065231, and 2017M3A9E9072669 to HRK) and the Institute for Basic Science (IBS-R013-A1 to DH). This study was also supported by a grant from Ministry of Food and Drug Safety (18182MFDS408 to SJH) and KBRI basic research program through Korea Brain Research Institute funded by Korean MSIT (19-BR-03-02 to SHC). BRL, JM, MJK, and BL are fellowship awardee by BK21 PLUS program.

Address correspondence to: Sang-Jun Ha, 50 Yonsei-ro, Seodaemun-gu, Seoul 03722, Republic of Korea. Phone: 82.2.2123.2696; Email. sjha@yonsei.ac.kr. Or to: Hye Ryun Kim, 50-1 Yonsei-ro, Seodaemun-gu, Seoul 03722, Republic of Korea. Phone: 82.2.2228.0831; Email: nobelg@yuhs.ac. Or to: Daehee Hwang, 1 Gwanak-ro, Gwanak-gu, Seoul 08826, Republic of Korea. Phone: 82.2.880.7522; Email: dhwang@snu.ac.kr.

1. Beatty GL, Gladney WL. Immune escape mechanisms as a guide for cancer immunotherapy. *Clin Cancer Res*. 2015;21(4):687–692.
2. Topalian SL, Drake CG, Pardoll DM. Immune checkpoint blockade: a common denominator approach to cancer therapy. *Cancer Cell*. 2015;27(4):450–461.
3. Sharma P, Hu-Lieskovan S, Wargo JA, Ribas A. Primary, Adaptive, and Acquired Resistance to Cancer Immunotherapy. *Cell*. 2017;168(4):707–723.
4. Gibney GT, Weiner LM, Atkins MB. Predictive biomarkers for checkpoint inhibitor-based immunotherapy. *Lancet Oncol*. 2016;17(12):e542–e551.
5. Sunshine J, Taube JM. PD-1/PD-L1 inhibitors. *Curr Opin Pharmacol*. 2015;23:32–38.
6. Chae YK, et al. Biomarkers for PD-1/PD-L1 Blockade Therapy in Non-Small-cell Lung Cancer: Is PD-L1 Expression a Good Marker for Patient Selection? *Clin Lung Cancer*. 2016;17(5):350–361.
7. Jiang P, et al. Signatures of T cell dysfunction and exclusion predict cancer immunotherapy response. *Nat Med*. 2018;24(10):1550–1558.
8. Kroemer G, Zitvogel L. Cancer immunotherapy in 2017: The breakthrough of the microbiota. *Nat Rev Immunol*. 2018;18(2):87–88.
9. Rizvi NA, et al. Cancer immunology. Mutational landscape determines sensitivity to PD-1 blockade in non-small cell lung cancer. *Science*. 2015;348(6230):124–128.
10. Zarour HM. Reversing T-cell Dysfunction and Exhaustion in Cancer. *Clin Cancer Res*. 2016;22(8):1856–1864.
11. Anderson AC, Joller N, Kuchroo VK. Lag-3, Tim-3, and TIGIT: Co-inhibitory Receptors with Specialized Functions in Immune Regulation. *Immunity*. 2016;44(5):989–1004.
12. Fourcade J, et al. PD-1 and Tim-3 regulate the expansion of tumor antigen-specific CD8+ T cells induced by melanoma vaccines. *Cancer Res*. 2014;74(4):1045–1055.
13. Chauvin JM, et al. TIGIT and PD-1 impair tumor antigen-specific CD8+ T cells in melanoma patients. *J Clin Invest*. 2015;125(5):2046–2058.
14. Sakuishi K, Apetoh L, Sullivan JM, Blazar BR, Kuchroo VK, Anderson AC. Targeting Tim-3 and PD-1 pathways to reverse T cell exhaustion and restore anti-tumor immunity. *J Exp Med*. 2010;207(10):2187–2194.

15. Johnston RJ, et al. The immunoreceptor TIGIT regulates antitumor and antiviral CD8(+) T cell effector function. *Cancer Cell*. 2014;26(6):923–937.
16. Chihara N, et al. Induction and transcriptional regulation of the co-inhibitory gene module in T cells. *Nature*. 2018;558(7710):454–459.
17. Cancer Genome Atlas Research Network. Comprehensive molecular profiling of lung adenocarcinoma. *Nature*. 2014;511(7511):543–550.
18. Rousseaux S, et al. Ectopic activation of germline and placental genes identifies aggressive metastasis-prone lung cancers. *Sci Transl Med*. 2013;5(186):186ra66.
19. Botling J, et al. Biomarker discovery in non-small cell lung cancer: integrating gene expression profiling, meta-analysis, and tissue microarray validation. *Clin Cancer Res*. 2013;19(1):194–204.
20. Okayama H, et al. Identification of genes upregulated in ALK-positive and EGFR/KRAS/ALK-negative lung adenocarcinomas. *Cancer Res*. 2012;72(1):100–111.
21. Kuner R, et al. Global gene expression analysis reveals specific patterns of cell junctions in non-small cell lung cancer subtypes. *Lung Cancer*. 2009;63(1):32–38.
22. Hunter JE, Schmidt FL. *Methods of Meta-analysis: correcting error and bias in research findings*. Sage; 1990.
23. Herbst RS, et al. Pembrolizumab versus docetaxel for previously treated, PD-L1-positive, advanced non-small-cell lung cancer (KEYNOTE-010): a randomised controlled trial. *Lancet*. 2016;387(10027):1540–1550.
24. Lau J, et al. Tumour and host cell PD-L1 is required to mediate suppression of anti-tumour immunity in mice. *Nat Commun*. 2017;8:14572.
25. Noguchi T, et al. Temporally Distinct PD-L1 Expression by Tumor and Host Cells Contributes to Immune Escape. *Cancer Immunol Res*. 2017;5(2):106–117.
26. Juneja VR, et al. PD-L1 on tumor cells is sufficient for immune evasion in immunogenic tumors and inhibits CD8 T cell cytotoxicity. *J Exp Med*. 2017;214(4):895–904.
27. Zhang Q, et al. Blockade of the checkpoint receptor TIGIT prevents NK cell exhaustion and elicits potent anti-tumor immunity. *Nat Immunol*. 2018;19(7):723–732.
28. Nakai R, et al. Overexpression of Necl-5 correlates with unfavorable prognosis in patients with lung adenocarcinoma. *Cancer Sci*. 2010;101(5):1326–1330.
29. Guo X, et al. Global characterization of T cells in non-small-cell lung cancer by single-cell sequencing. *Nat Med*. 2018;24(7):978–985.
30. Hsu J, et al. Contribution of NK cells to immunotherapy mediated by PD-1/PD-L1 blockade. *J Clin Invest*. 2018;128(10):4654–4668.
31. Leach DR, Krummel MF, Allison JP. Enhancement of antitumor immunity by CTLA-4 blockade. *Science*. 1996;271(5256):1734–1736.
32. Kamphorst AO, et al. Rescue of exhausted CD8 T cells by PD-1-targeted therapies is CD28-dependent. *Science*. 2017;355(6332):1423–1427.
33. Hui E, et al. T cell costimulatory receptor CD28 is a primary target for PD-1-mediated inhibition. *Science*. 2017;355(6332):1428–1433.
34. Li XY, et al. CD155 loss enhances tumor suppression via combined host and tumor-intrinsic mechanisms. *J Clin Invest*. 2018;128(6):2613–2625.
35. Kong Y, et al. T-Cell Immunoglobulin and ITIM Domain (TIGIT) Associates with CD8+ T-Cell Exhaustion and Poor Clinical Outcome in AML Patients. *Clin Cancer Res*. 2016;22(12):3057–3066.
36. He W, et al. CD155T/TIGIT Signaling Regulates $CD8^+$ T-cell Metabolism and Promotes Tumor Progression in Human Gastric Cancer. *Cancer Res*. 2017;77(22):6375–6388.
37. Kurtulus S, et al. TIGIT predominantly regulates the immune response via regulatory T cells. *J Clin Invest*. 2015;125(11):4053–4062.
38. Golan T, et al. Phase 1 dose-finding study of the anti–TIGIT antibody MK-7684 as monotherapy and in combination with pembrolizumab in patients with advanced solid tumors. Abstract presented at Society for Immunotherapy of Cancer (SITC) 33rd Annual Meeting; November 7–11, 2018; Washington, DC, USA. https://sitc.sitcancer.org/2018/abstracts/titles/?category=-Combination+Therapy.
39. Yonesaka K, et al. B7-H3 Negatively Modulates CTL-Mediated Cancer Immunity. *Clin Cancer Res*. 2018;24(11):2653–2664.
40. De Henau O, et al. Overcoming resistance to checkpoint blockade therapy by targeting PI3Kγ in myeloid cells. *Nature*. 2016;539(7629):443–447.
41. Davis RJ, et al. Anti-PD-L1 Efficacy Can Be Enhanced by Inhibition of Myeloid-Derived Suppressor Cells with a Selective Inhibitor of PI3Kδ/γ. *Cancer Res*. 2017;77(10):2607–2619.
42. Mariathasan S, et al. TGFβ attenuates tumour response to PD-L1 blockade by contributing to exclusion of T cells. *Nature*. 2018;554(7693):544–548.
43. Carbone DP, et al. First-Line Nivolumab in Stage IV or Recurrent Non-Small-Cell Lung Cancer. *N Engl J Med*. 2017;376(25):2415–2426.
44. Hellmann MD, et al. Tumor Mutational Burden and Efficacy of Nivolumab Monotherapy and in Combination with Ipilimumab in Small-Cell Lung Cancer. *Cancer Cell*. 2018;33(5):853–861.e4.
45. Bolstad BM, Irizarry RA, Astrand M, Speed TP. A comparison of normalization methods for high density oligonucleotide array databased on variance and bias. *Bioinformatics*. 2003;19(2):185–193.
46. Daniel WW. 9.1: Spearman Rank Correlation Coefficient and 9.2: Kendall's Tau. In: *Applied Nonparametric Statistics*. 2nd ed. PWS-Kent; 1990:358–365.
47. Kaplan EL, Meier P. Nonparametric estimation from incomplete observations. *J Amer Statist Assoc*. 1958;53(282):457–481.
48. Hirsch FR, et al. PD-L1 Immunohistochemistry Assays for Lung Cancer: Results from Phase 1 of the Blueprint PD-L1 IHC Assay Comparison Project. *J Thorac Oncol*. 2017;12(2):208–222.
49. Brahmer J, et al. Nivolumab versus Docetaxel in Advanced Squamous-Cell Non-Small-Cell Lung Cancer. *N Engl J Med*. 2015;373(2):123–135.
50. Dong H, Zhu G, Tamada K, Flies DB, van Deursen JM, Chen L. B7-H1 determines accumulation and deletion of intrahepatic CD8(+) T lymphocytes. *Immunity*. 2004;20(3):327–336.